THE JOURNAL OF PHYSICAL CHEMISTRY C
A JOURNAL OF THE AMERICAN CHEMICAL SOCIETY

pubs.acs.org/JPCC

Article

Aligned Organic Molecular Wires in Methionine Nanofilm Growth on Si(111)-$\sqrt{3}\times\sqrt{3}$-Ag

Hanieh Farkhondeh, Fatemeh R. Rahsepar, Lei Zhang, and Kam Tong Leung*

Cite This: *J. Phys. Chem. C* 2021, 125, 4223–4234

Read Online

ACCESS | Metrics & More | Article Recommendations | Supporting Information

ABSTRACT: Interfacial interactions of biomolecular materials with semiconductor surfaces have been of immense interest because of their technological applications in biosensors and biomolecular nanoelectronics. The fabrication of highly ordered, extended low-dimensional molecular patterns on Si surfaces promises to be an important breakthrough in the field of Si-based biomolecular nanodevices. Even though these remarkable biomolecular self-assemblies have been more often observed on metal surfaces, there are fewer relevant studies on Si surfaces because of the high reactivity of their dangling bonds. On the other hand, the presence and indeed the saturation of these dangling bonds provide a unique approach to engineer robust supramolecular architectures on these surfaces. In the present work, methionine nanofilm growth on a benchmark metal silicide surface, Si(111)-$\sqrt{3}\times\sqrt{3}$-Ag, at room and lower temperature has been investigated by X-ray photoelectron spectroscopy and scanning tunneling microscopy. Our results show the formation of extended one-dimensional molecular wires consisting of methionine dimer rows with zwitterionic intermolecular interactions similar to those observed on single-crystal metal surfaces. Notable surface defects such as step edges and antiphase boundaries are found to play a crucial role in the initiation and directed growth of the adsorption structures, while terrace sites appear to be more conducive to the development of aligned one-dimensional (nanowires, nanoboomerangs) and two-dimensional (nanogratings, and concentric nanotriangles) self-organized nanostructures. Our complementary density functional theory calculations further provide plausible adsorption configurations of individual molecular adspecies and self-organized oriented molecular wires on the terraces of the surface. We further illustrate the importance of molecule−molecule and molecule−substrate interactions that give rise to key differences between methionine adsorption arrangements on bare Si and the silver silicide surfaces.

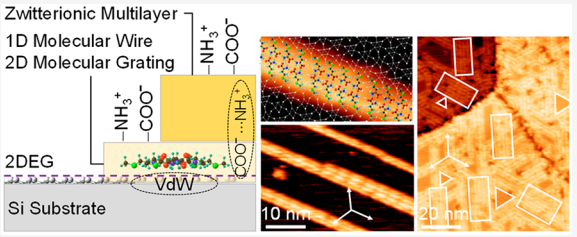

1. INTRODUCTION

Understanding the interactions between biomolecules and solid surfaces on the atomic scale and the mechanism of nanofilm growth is of paramount importance to not just expanding our basic knowledge about biological materials but also enabling technological applications that exploit hybrid organic−inorganic structures in the design of next-generation catalysts, biosensors, and nanoelectronic devices. The adsorption of biomolecules on metal and semiconductor surfaces has been studied extensively because of their applications enabled particularly by surface functionalization and molecular self-assembly.[1] Detailed understanding of the physical and chemical phenomena at the interface between biomolecules and the solid surface could lead to better control of the self-organization processes, which is important for the synthesis of multifunctional materials based on two-dimensional nanostructures and the development of promising biocompatible nanomaterials and devices. Not surprisingly, bio-organic molecules such as amino acids play a particularly important role in these fields. As the smallest building blocks of peptides and proteins, amino acids are among the most fundamental benchmark systems for elucidating the interactions of more complex bio-organic molecules with surfaces. In addition to powerful chemical and physical properties, they also offer potential biological functionalities, which make them excellent candidates for functionalization of solid surfaces, often serving as the first step in building a biocatalyst or a bioactive or sensing device.

Of the 20 proteinogenic amino acids (that are used in the genetic code), methionine is one of two sulfur-containing amino acids and the only one with a methylthiomethylene end group. Methionine is important to molecular biosynthesis in the human body, and because of its antioxidant properties, it is known to prevent cell damage resulting from cancer treatments without delaying antitumor activity.[2] The ability of methionine to self-assemble on metal surfaces offers a promising approach for the design of drug delivery carriers and bioarchitectures with customizable nanostructures. Fundamental understanding

Received: November 20, 2020
Revised: January 13, 2021
Published: February 10, 2021

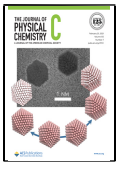

https://dx.doi.org/10.1021/acs.jpcc.0c10470
J. Phys. Chem. C 2021, 125, 4223−4234

of its self-assembly properties on metal surfaces is therefore of particular interest. Among the large volume of research on benchmark amino acids on metal surfaces,[1] only a few studies have focused on methionine, despite the aforementioned potential applications. In particular, two-dimensional molecularly ordered structures of L-methionine have been reported to form on Ag(111), and holding the substrate surface at 320 K during deposition has been used to promote the formation of regularly spaced gratings.[3] On Au(111), D- and L-methionine have been found to form parallel chains or "ziplike" dimer rows in the formation of hydrogen-bonded zwitterionic layers at room temperature.[4,5] Furthermore, steering of the chiral organization of L-methionine on Cu(111)[6] has been shown to be strongly affected by the substrate reactivity and thermal activity.

The configuration of a stable two-dimensional structure at thermodynamic equilibrium can be controlled by not only the lateral interactions among the adsorbates but also the nature of the chemical and structural characteristics of the underlying support. In our previous work, the formation of self-organized methionine trimers on a Si(111)7×7 surface at room temperature was found to be governed by the N−Si covalent bonding at the center adatoms of the 7×7 surface and by the intermolecular hydrogen bonding that leads to the formation of Y-shaped trimers.[7] While the two-dimensional electron gas of a metallic surface facilitates fast diffusion of organic molecules and hence promotes the fabrication of molecular self-assembled structures,[8] the strong directional dangling bonds of a semiconductor surface [such as Si(111)7×7] favor trapping of molecules in a diffusion-limited condition, thereby potentially inhibiting the long-range self-assembly of small amino acids. One advantage of these fundamentally interesting Si-based substrates over metal substrates is that they are essential for fabricating electronic devices by large-scale integration techniques. Passivation of Si surfaces with metal atoms offers a promising approach for altering the surface diffusion properties of the adsorbed molecules and hence promoting the formation of the equilibrium state of self-assembled molecular structures. Among all metal-passivated Si surfaces, Si(111)-$\sqrt{3}\times\sqrt{3}$-Ag is one of the most studied prototypical metal−semiconductor interfaces.[9] It is formed by deposition of one monolayer of Ag atoms on the Si(111) surface followed by annealing at an elevated temperature. The parabolic surface band structure of Si(111)-$\sqrt{3}\times\sqrt{3}$-Ag near the Fermi level resembles that of a typical metal surface.[10−12] Although the properties of the Si(111)-$\sqrt{3}\times\sqrt{3}$-Ag surface are more similar to those of metal surfaces than Si surfaces, there are also significant structural differences in the sizes of their unit cells and in the Ag−Ag surface separations. Furthermore, while the topmost layer of the Si(111)-$\sqrt{3}\times\sqrt{3}$-Ag surface is composed of Ag atoms, the underlying layers are composed of Si atoms, which leads to surface electronic states containing Ag−Si components, as opposed to the Ag−Ag surface states on the Ag(111) surface.

Physisorption of numerous organic molecules on the Si(111)-$\sqrt{3}\times\sqrt{3}$-Ag surface has been studied, mostly at room temperature. These organic molecules include cobalt phthalocyanine,[13] fullerenes,[14] perylene tetracarboxylic diimide (PTCDI),[15] pentacene,[16] trimesic acid,[17] cyanuric acid−melamine,[18] adenine,[19] 3,4,9,10-perylene tetracarboxylic dianhydride (PTCDA),[20] nickel(II) porphine,[21] 5,10,15,20-tetrakis(4-bromophenyl)porphyrin−Co,[22] α-sexithiophene,[23] and halogenated oligothiophenes.[24] All of these studies have focused on the adsorption and formation of organic molecular films. There is only one report on the substrate effect, in which scanning tunneling microscopy (STM) was used to illustrate the effects of three different substrates, Si(111)7×7, Ag(111), and Si(111)-$\sqrt{3}\times\sqrt{3}$-Ag, on the structural formation of the terephthalic acid and metal−organic framework, with the goal of understanding how passivated semiconductor surfaces differ from the semiconductor and metal surfaces.[25] Indeed, the Si(111)-$\sqrt{3}\times\sqrt{3}$-Ag surface has been found to behave more like Ag(111) in terms of mediating the formation of supramolecular structures. The reactivities of these three surfaces were observed to follow the general trend Si(111) (most reactive) > Si(111)-$\sqrt{3}\times\sqrt{3}$-Ag > Ag(111) (least reactive). In our recent study, we investigated the chemisorption of cysteine, the only thiol-containing amino acid, on Si(111)-$\sqrt{3}\times\sqrt{3}$-Ag.[26] As the thiol end group in cysteine is replaced by the methylthiomethylene end group in methionine, methionine is a more suitable candidate for the formation of physisorbed supramolecular architectures because the methylthiomethylene group is less reactive with the substrate, thereby accentuating more intermolecular interactions.

In this work, we investigate the viability of the two-dimensional metal silicide surface Si(111)-$\sqrt{3}\times\sqrt{3}$-Ag in the formation of low-dimensional molecular structures. We study the interface and growth properties of methionine from submonolayer to multilayer coverages on Si(111)-$\sqrt{3}\times\sqrt{3}$-Ag at room temperature. Our goal is to determine the changes in the chemical states of methionine at notable adsorption sites of this popular Ag silicide surface. Our combined data provided by X-ray photoelectron spectroscopy (XPS) and STM offer a comprehensive picture of the nature of molecule−molecule and molecule−substrate interactions at the interface and during the early growth stage. These data are supported by complementary quantum-mechanical calculations based on density functional theory (DFT) with van der Waals corrections (D2). These calculations have enabled us to identify the chemical states of the adspecies and their most probable adsorption configurations as well as plausible one-dimensional and two-dimensional self-assembled nanostructures on the surface. In addition, we compare the adsorption properties of methionine on Si(111)-$\sqrt{3}\times\sqrt{3}$-Ag with those on its "parent" surfaces, Si(111)7×7 and Ag(111). Structural correlation with the $\sqrt{3}\times\sqrt{3}$-Ag surface is found to be particularly important to the formation of self-organized low-dimensional patterns of aligned molecular wires.

2. EXPERIMENTAL AND COMPUTATIONAL DETAILS

All of the experiments were performed in a five-chamber ultrahigh-vacuum system (Omicron Nanotechnology, Inc.) with a base pressure better than 5×10^{-11} mbar. Surface characterizations were carried out in the analysis chamber, which was equipped with an X-ray photoelectron spectrometer and a variable-temperature scanning tunneling microscope. The XPS spectrometer consisted of a SPHERA hemispherical analyzer, a seven-channeltron detector, and a monochromatic Al Kα source. An electrochemically etched atomically sharp W tip was used to scan the electronic structure of the surface. The STM measurements were performed with a constant current of 0.2 nA and, with the tip grounded, a bias voltage of −2 V applied to the sample for filled-state imaging or +2 V for empty-state imaging. A single-side-polished n-type Si(111) chip (11×2 mm^2 in size and 0.3 mm thick) with a resistivity of 5 mΩ cm (Virginia Semiconductor, Inc.) was used as the

https://dx.doi.org/10.1021/acs.jpcc.0c10470
J. Phys. Chem. C 2021, 125, 4223−4234

substrate. The Si chip was first cleaned with acetone and isopropanol in an ultrasound cleaner and then introduced into the analysis chamber, where it was thoroughly degassed by direct-current annealing at 400 °C for 12 h. An atomically clean Si(111)7×7 surface was obtained by repeated flash-annealing, in which the degassed sample was heated rapidly to 1200 °C and slowly cooled to room temperature. The Si(111)-$\sqrt{3}\times\sqrt{3}$-Ag surface was prepared in a separate molecular beam epitaxy (MBE) chamber by deposition of silver from a high-temperature effusion cell (Dr. Ebert MBE-Komponenten GmbH) held at 870 °C onto the clean Si(111)7×7 surface (held at room temperature) followed by direct-current annealing to 500 °C for 120 s.[27] The quality of both the Si(111)7×7 surface before Ag deposition and the resulting Si(111)-$\sqrt{3}\times\sqrt{3}$-Ag surface was then verified by STM and XPS before deposition of methionine. Methionine in a low-temperature organic effusion cell (Dr. Ebert MBE-Komponenten GmbH) was evaporated onto the substrate in another separate MBE chamber. Before methionine exposure, the purity of the methionine powder was verified in situ using a quadrupole mass spectrometer (Stanford Research Systems RGA-300), and the monitored cracking pattern was found to be in good accord with the literature.[28] Methionine (99.5% purity, Fluka) films of submonolayer to multilayer coverages were prepared with the effusion cell temperature set to 120 °C during exposure of the methionine vapor to the Si(111)-$\sqrt{3}\times\sqrt{3}$-Ag surface held at room temperature for different exposure times, during which the background pressure of this MBE chamber was 2×10^{-9} mbar. All of the XPS experiments were conducted with the sample held at room temperature, while the STM experiments were carried out both at room temperature and at low temperature. The XPS spectra were recorded at a pass energy of 20 eV with an energy resolution of 0.7 eV full width at half-maximum (fwhm) for the Ag $3d_{5/2}$ photoline at 368.3 eV. The Casa XPS software was used to fit the spectra with Gaussian−Lorentzian (GL30) line shapes after appropriate correction for the Shirley background. The STM image analyses were performed by using the WSXM software.[29]

The first-principles DFT calculations were carried out using the Vienna Ab Initio Simulation Package (VASP), version 5.4, with the Materials Exploration and Design Analysis (MedeA) platform, version 2.19 (Materials Design, Inc.). The projector augmented wave (PAW) method[30,31] was used to describe the electron−ion interactions. The generalized gradient approximation (GGA) with the Perdew−Burke−Ernzerhof (PBE) exchange−correlation functional was used.[32] The Brillion zone was sampled at the Γ point with a **k**-point spacing of 0.5 $Å^{-1}$. A cutoff energy of 400 eV was used for the convergence of the plane-wave expansion. As our system involves interactions of organic molecules, dispersion forces were included in the calculations. For that purpose, we employed the Grimme D2 method,[33] implemented in VASP as the DFT-D2 force field. DFT-D2 describes the van der Waals interactions for an atom with its neighbors in a given radius via a simple pairwise force field. The calculated dispersion energy is summed with the conventional Kohn−Sham DFT energy in the results. The conjugate-gradient algorithm was used to optimize the ionic geometry. The honeycomb-chained-trimer model was employed to describe the Si(111)-$\sqrt{3}\times\sqrt{3}$-Ag substrate. The slab contained three Si double layers (with a lattice constant of 5.41 Å), one Ag−Si trimer layer (as the topmost layer), and one H layer (as the bottom layer for termination of the bottom-most silicon layer to simulate continuation to the Si bulk structure). The periodic supercell was composed of 4×4 = 16 unit cells for monomer and dimer methionine adsorption or 8×4 = 32 unit cells of Si(111)-$\sqrt{3}\times\sqrt{3}$-Ag for methionine nanowire formation with a vacuum gap of 10 Å in the z direction. The adsorption energy (E_{ads}) was calculated using the following equation:

$$E_{ads} = (E_{sys} - nE_{met} - E_{slab})/n$$

where n is the number of methionine molecules in the cell, E_{sys} is the total energy of the (adsorbate + surface) system, and E_{met} and E_{slab} are the total energies of the single methionine molecule and the surface slab obtained after separate geometry optimization, respectively.

3. RESULTS AND DISCUSSION

3.1. Evolution of Chemical State Composition during Methionine Film Growth at Room Temperature. Like all other proteinogenic amino acids, methionine is found in a neutral form in the gas phase and a zwitterionic form in the liquid and solid phases. Scheme 1 shows ball-and-stick models

Scheme 1. Ball-and-Stick Models of the Isolated Structures of a Methionine Molecule in (a) Neutral and (b) Zwitterionic Forms[a]

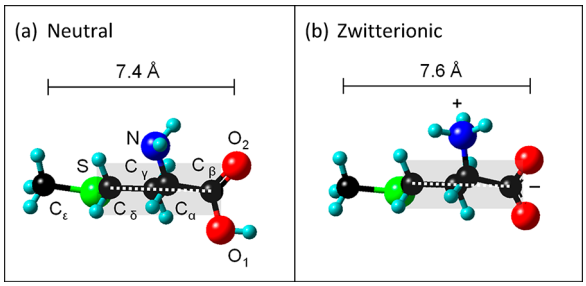

[a]The models were generated by DFT-D2 calculations. In our notation, we identify −COOH as the "head" group and the functional group farthest from the head group as the "tail" group. The long axis (starting from the head group) is marked by a dashed line, while the molecular plane containing the long axis and the −COO moiety is identified by a shaded rectangle.

of the neutral and zwitterionic forms of the methionine molecule. The difference between methionine and cysteine, the only two S-containing amino acids, is that the thiol group (−SH) in cysteine ($HOOC_\beta C_\alpha H(NH_2)C_\gamma H_2\mathbf{SH}$) is replaced by a methylthiomethylene group ($-CH_2SCH_3$) in methionine ($HOOC_\beta C_\alpha H(NH_2)C_\gamma H_2\mathbf{C}_\delta\mathbf{H}_2\mathbf{SC}_\varepsilon\mathbf{H}_3$). The carbon chain backbone contains four C atoms in methionine (without the $-SC_\varepsilon H_3$ moiety) and three C atoms in cysteine (without the −SH group), and the molecular length of methionine is 1.5 times that of cysteine. The termination of the S atom by a methyl group in the methylthiomethylene group also makes methionine less reactive than cysteine (with the highly reactive thiol group).

Figure 1 shows the O 1s, N 1s, C 1s, and S 2s spectra of methionine as functions of exposure time on Si(111)-$\sqrt{3}\times\sqrt{3}$-Ag at room temperature. The corresponding peak positions and assignments obtained for the fitted features are summarized in Table S1, while the changes in their relative intensities are given in Figure S1. Increasing the exposure time from 120 to 360 s generally increases the intensities of all of

https://dx.doi.org/10.1021/acs.jpcc.0c10470
J. Phys. Chem. C 2021, 125, 4223−4234

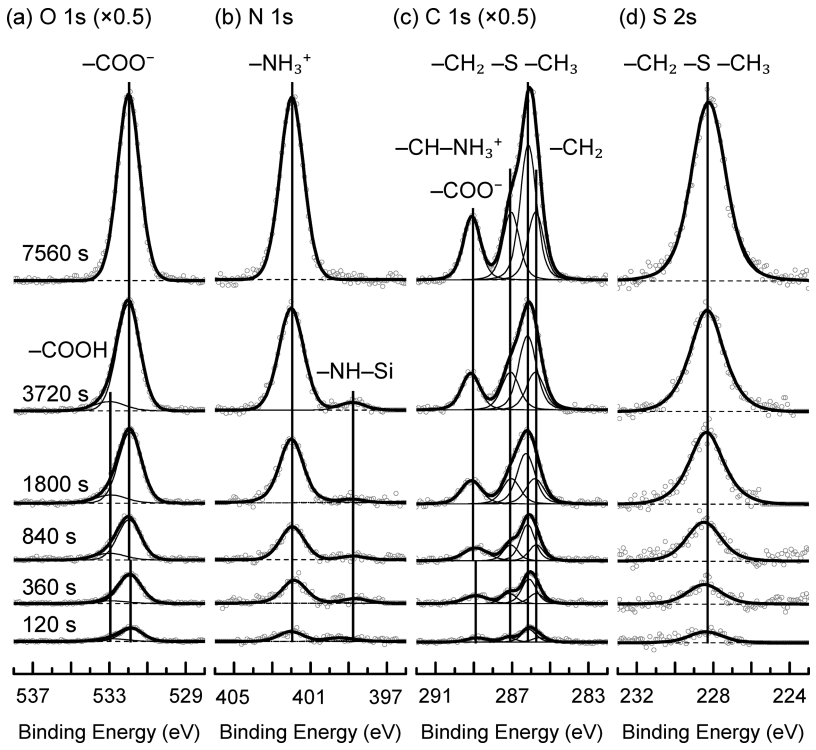

Figure 1. Evolution of the (a) O 1s, (b) N 1s, (c) C 1s, and (d) S 2s XPS spectra of methionine deposited on Si(111)-$\sqrt{3}\times\sqrt{3}$-Ag as functions of exposure time (120−7560 s).

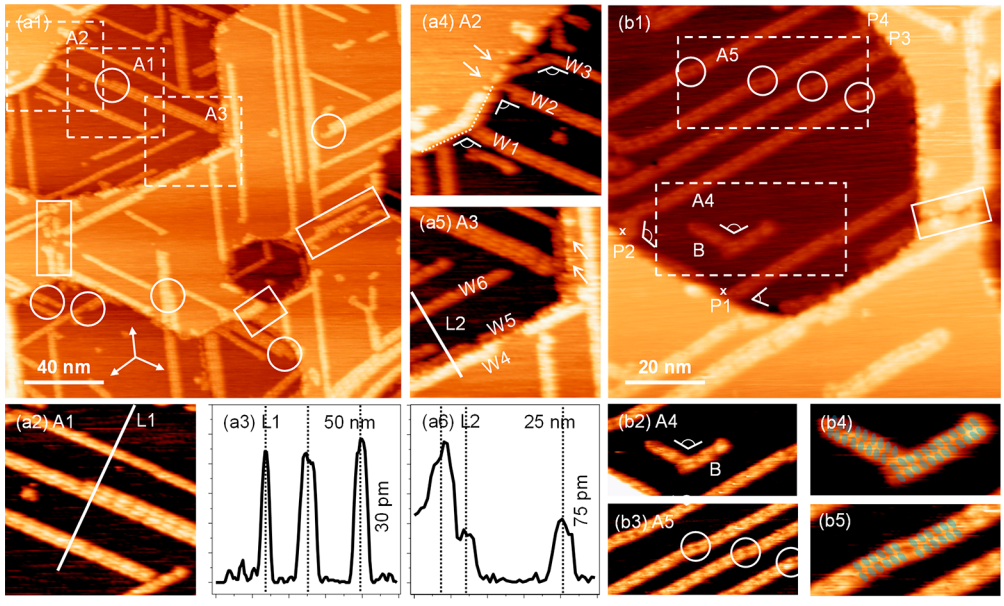

Figure 2. Empty-state STM images of a 30 s exposure of L-methionine to Si(111)-$\sqrt{3}\times\sqrt{3}$-Ag over (a1) a 200×200 nm^2 scan area and (b1) a selected 100×100 nm^2 area at a higher magnification. Expanded views with modified image contrasts of the selected areas (A1, A2, A3) in (a1) and (A4, A5) in (b1) are shown to illustrate (a2) the emergence of the dimer rows in A1, (a4) directed growth from the step edges in A2, (a5) parallel growth along the step edges in A3, (b2) a "boomerang" nanostructure in A4, and (b3) kinks in the individual lines in a nanograting in A5. The respective apparent height profiles along line L1 in (a2) and line L2 in (a5) are shown in (a3) and (a6), respectively. (b4) and (b5) show schematic diagrams of dimer rows superimposed on the corresponding STM images of the respective boomerang nanostructure in (b2) and kink structure in (b3). The STM images were obtained with a sample bias of +2.0 V and a tunneling current of 0.2 nA with the sample held at 140 K.

the components in the XPS region spectra (Figure 1). The predominant N 1s peak at 401.8 eV can be assigned to the protonated amino group, while the weak N 1s feature at 398.7 eV is in good agreement with the N−Si linkage reported for methionine adsorbed on the Si(111)7×7 surface.[7,34] Formation of the N−Si bond could arise from N−H dissociative adsorption of methionine at defect sites such as step edges and antiphase boundaries of the Si(111)-$\sqrt{3}\times\sqrt{3}$-Ag surface. The O 1s spectra can be fitted with a main peak at 531.8 eV assigned to the deprotonated carboxylic acid group and a weaker one at 532.7 eV assigned to the neutral carboxylic acid group.[35] This latter feature likely corresponds to the adsorbed

https://dx.doi.org/10.1021/acs.jpcc.0c10470
J. Phys. Chem. C 2021, 125, 4223−4234

species at defect sites. The single S 2s peak located at 228.4 eV can only be attributed to the sulfur atom in the methylthiomethylene group. The four C 1s features at 285.5, 285.9, 286.9, and 288.7 eV can be assigned to $-CH_2$, $-CH_2-S-CH_3$, $-CH-NH_3^+$, and $-COO^-$, respectively, with atomic ratios of 1:2:1:1, in accordance with the stoichiometric composition of zwitterionic methionine adspecies. Indeed, the presence of the deprotonated carboxylic acid group ($-COO^-$) and protonated amino group ($-NH_3^+$) along with the intact methylthiomethylene group indicates nondissociative adsorption of methionine in its zwitterionic state. Physisorption of zwitterionic methionine on the Ag(111)[3] and Au(111)[4,5] surfaces has also been reported at cryogenic temperature and up to room temperature. On Cu(111),[6] methionine was found to adsorb in both anionic and zwitterionic states, while the adsorption state on the Cu(110) surface[36] is only anionic with a stronger Cu-to-O interaction.

Increasing the exposure time to 840, 1800, and 3720 s leads to further increases in the intensities of the peaks in all four regions without introducing any chemical shifts. The peak positions of XPS spectra for the methionine multilayer obtained for the 7560 s exposure to Si(111)-$\sqrt{3}\times\sqrt{3}$-Ag are found to be similar to those for the methionine powder in the solid phase.[37] Comparing the XPS spectra of the methionine multilayer with those of the lower exposures shows that intermolecular zwitterionic interactions are clearly present even at the lowest coverage (120 s exposure). Most of the adsorbate species are therefore physisorbed on the surface, as no significant chemical shifts in the dominant peaks of all regions are observed. Indeed, only a small fraction of the adsorbates are found to be chemisorbed, most likely at defect sites through N−H bond cleavage.

3.2. Formation of Methionine Molecular Wires on Si(111)-$\sqrt{3}\times\sqrt{3}$-Ag in the Early Growth Stage. In order to take advantage of the well-defined $\sqrt{3}\times\sqrt{3}$-Ag overlayer as a reference template on Si(111), we focus our STM studies on the early growth stage of the methionine film. A pristine Si(111)-$\sqrt{3}\times\sqrt{3}$-Ag surface is generally found to contain both lower-step terraces (darker areas) and upper-step terraces (brighter areas).[38,39] STM measurements of a low exposure (e.g., 120 s) of methionine to Si(111)-$\sqrt{3}\times\sqrt{3}$-Ag performed both at room temperature (Figure S2) and at low temperature (see Figure 3 below) generally show that the molecular adsorption patterns are very similar at the two temperatures. However, the bright protrusion features in both the lower-step terraces and upper-step terraces obtained at room temperature appear more diffuse, which could be attributed to the higher mobility and faster surface diffusion of methionine molecules at room temperature compared with low temperature.

To mitigate the effect of surface diffusion so that we can investigate these organized adsorbate nanostructures in more detail, we focus on our low-temperature STM results. Figure 2a1 shows the STM image of the surface after a 30 s exposure of methionine (at room temperature) collected with the surface held at 140 K. Unlike cysteine, methionine forms well-defined one-dimensional extended ordered structures with distinct widths. The one-dimensional extended molecular stripes are formed on the surface terraces with three distinct orientations that are 120° from one another. Interestingly, a large number of these stripes tend to align in parallel with the step-edge directions. As the step-edge directions are known to be along the $\langle 110\rangle$ and $\langle 11\bar{2}\rangle$ directions,[38] the orientations of these molecular wires are likely along these same directions. In our room-temperature STM measurements shown in Figure S3, the atomically resolved image of the underlying $\sqrt{3}\times\sqrt{3}$-Ag electronic structure in the vicinity of the as-formed methionine stripes can be obtained. Using the substrate grid as the reference, this result evidently identifies the orientations of the molecular stripes to be mainly along the close-packed $\langle 11\bar{2}\rangle$ rows of the Si(111)-$\sqrt{3}\times\sqrt{3}$-Ag surface. In a few regions, however, the molecular stripes appear to be rotated slightly by 11±2° clockwise with respect to the $\langle 11\bar{2}\rangle$ direction. This could result from an adjustment of the molecular adsorption sites in the stripes to maximize the molecule−molecule interactions (discussed further in section 3.4 below). Interestingly, these deviations from the surface close-packed orientations are rarely observed in our low-temperature STM results, suggesting that the effects of the molecule−substrate interactions are weaker at room temperature than at low temperature.

As illustrated in area A1 (Figure 2a1,a2) and the corresponding height profile along line L1 (Figure 2a3), the molecular wires appear to have three different widths: 1.9, 3.4, and 4.7 nm. The width of the thinnest molecular wire is close to that of a methionine dimer with a head-to-head configuration (discussed further below) and is in good accord with the observation of one-dimensional extended structures of methionine on Ag(111).[3] Considering the theoretical width of a model dimer to be 1.5 nm, the widths of the molecular wires are found to be 1.2, 2.3, and 3.1 times that of a model dimer. In other words, the thicker stripes can be considered as two or three such molecular wires lying side by side next to each other. The open circles in Figure 2a1 mark the edges of the single dimer rows grown next to another molecular wire, creating thicker stripes. This "bundling" of multiple molecular wires into stripes with integral widths is clearly observed in Figure 2a2 and the corresponding height profile along line L1 (Figure 2a3), which show from top to bottom single, triple, and double dimer rows. Furthermore, there appears to be an interstripe surface-mediated long-range interaction that leads to one-dimensional extended ordering among a number of stripes with well-defined interstripe spacings between them. Figure 2a2 shows an example of such interactions with interstripe spacings of 8.3 and 10.4 nm. However, the long-range order is disrupted occasionally when another stripe with a different orientation starts to grow nearby, which leads to the formation of interstripe joints with 60° and 120° angles.

A similar type of linear structures has been observed on the Ag(111) surface,[3,40] where aligned one-dimensional structures were extended on the large terraces with well-defined and equal interstripe separations. These Ag(111) STM data collected at 15 K showed that the so-called nanograting was stable up to room temperature, with molecular desorption occurring above 370 K. Formation of the one-dimensional molecular grating has also been reproduced on Cu(111) under ultrahigh-vacuum conditions[6] and on graphite under ambient conditions[41,42] at various temperatures up to room temperature. On Ag(111), the nanowires were oriented along the high-symmetry substrate directions, while on the more reactive Cu(111) surface the assembly of nanowires was found to align with an angle of −10° with respect to the $\langle 110\rangle$ axes below 273 K and +10° above 283 K. The small tilt of 10° in molecular ordering with respect to the atomic close-packed rows of the underlying substrate was thought to be related to the smaller lattice constant (and higher reactivity) of the Cu(111) substrate (2.55 Å) compared with the Ag(111)

https://dx.doi.org/10.1021/acs.jpcc.0c10470
J. Phys. Chem. C 2021, 125, 4223−4234

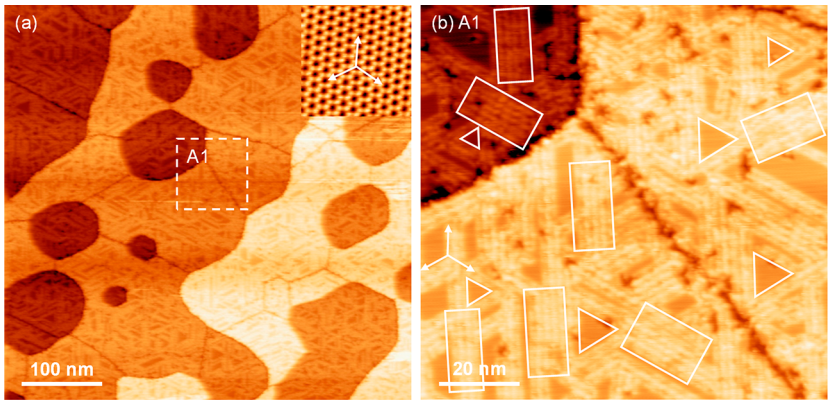

Figure 3. Empty-state STM images of a 120 s exposure of L-methionine on Si(111)-$\sqrt{3}\times\sqrt{3}$-Ag (a) over a 500×500 nm^2 scan area and (b) a selected 100×100 nm^2 area [area A1 in (a)]. The inset in (a) shows an atomic-resolution STM image of the pristine Si(111)-$\sqrt{3}\times\sqrt{3}$-Ag surface in approximately the same orientation as the substrate in (b), which illustrates the alignment of the molecular wires in nanogratings (marked by rectangles) and concentric triangular nanodomains (the centers of which marked by triangles) along the three equivalent crystallographic directions of the supporting Si(111)-$\sqrt{3}\times\sqrt{3}$-Ag surface. The STM images were obtained with a sample bias of +2.0 V and a tunneling current of 0.2 nA with the sample held at 140 K.

substrate (2.89 Å). These studies further proposed that a single nanowire corresponds to a dimer row of methionine molecules extended along a direction in registry with one of the substrate crystallographic directions. The dimerization was shown to be mediated by zwitterionic intermolecular hydrogen bonding of methionine on Ag(111) and by a combination of anionic and zwitterionic intermolecular bonding on Cu(111). The zwitterionic molecular dimerization leading to the formation of one-dimensional nanowires being commensurate with the underlying atomic lattice was also reported for L-tyrosine on Ag(111),[43] which has further been proposed as a "universal" bonding scheme for two-dimensional zwitterionic systems. Indeed, this bonding picture is consistent with our present STM images of methionine molecular wires on Si(111)-$\sqrt{3}\times\sqrt{3}$-Ag.

Unlike Ag(111) and other noble metal single-crystal surfaces, the presence of step edges and antiphase boundaries on the Si(111)-$\sqrt{3}\times\sqrt{3}$-Ag surface provides an opportunity to investigate any structural correlative effect on the formation of molecular wires exerted by these defect sites. Indeed, some of the molecular wires appear to nucleate at the step edges while others are formed on the surface terraces, where the number of molecular wires unattached to the step edges is evidently less than the number of attached ones. This confirms that while the formation of molecular wires can occur on the relatively defect-free terraces, nucleation at the step edges that leads to molecular wires is more probable. The higher likelihood of nucleation at the step edges could arise because molecules are trapped at these defect sites more easily than at the terrace sites. In Figure 2a4, the individual bright protrusions on the upper-step edge in area A2 (marked by arrows) can be attributed to single molecules and dimers, while the white stripe appears to resemble a dimer row along and conforming to the upper-step edge. A dashed line is drawn alongside the step edge to highlight the change in the step edge direction and to illustrate the close alignment of the molecular wire to the step edge. On the lower-step terrace shown in Figure 2a4, the molecular wires appear to originate from the kink (molecular wire W1) and from the straight part of the step edge (molecular wire W2). While the double dimer row in molecular wire W2 extends perpendicular to the step edge, W1 is directed 120° from the left side of the step edge and emerges perpendicular to the right side of the step edge. The lower-step edge sites between molecular wires W1 and W2 are filled with discrete bright protrusions, corresponding to individual dimer units that nucleate along a similar growth direction as W1 and W2. Originating at the lower-step edge as a single dimer row and grown with a 120° step-edge angle initially, molecular wire W3 then changes its growth path and becomes parallel to W1 and W2. All of the wires nucleated at the step edges extend further onto the terrace following the direction of the underlying $\sqrt{3}\times\sqrt{3}$-Ag template. Another adsorption morphology near the upper-step and lower-step edges is observed in area A3 (Figure 2a5). Near the upper-step edge, the single bright protrusions marked by arrows likely represent the single and dimer methionine adsorbates. The bright stripes running parallel along the upper-step edge (molecular wire W4) and lower-step edge (W5) are as wide as the single stripe on the lower-step terrace (W6), as shown in the height profile along line L2 (Figure 2a6). On the basis of their similar widths (1.9−2.1 nm), they can therefore be considered as single molecular wires.

Like the step edges, the antiphase boundaries also appear to confine the stripes, as supported by the presence of the stripes either formed parallel along or nucleated at and extended from an antiphase boundary, as shown in the regions marked by the open rectangles in Figure 2a1,b1. No molecular wires are found to grow across an antiphase boundary. Both step edges and antiphase boundaries provide favorable trapping sites for methionine because of their lower coordination numbers (as revealed in the perpendicular and 120° growth directions) and the perturbation of the electronic density of states, as manifested in the alignment of molecular wires along the step edges and antiphase boundaries (i.e., parallel growth).

Figure 2b1 shows an STM image of a typical nanoscale grating of dimer rows with well-defined width and spacing on a lower-step terrace. Similar gratings can also be found on the upper-step terraces. The nanograting arises as the result of collective alignment of the molecular wires in registry with the preferred crystallographic directions of the $\sqrt{3}\times\sqrt{3}$-Ag surface terraces. These molecular wires are found to originate from one edge of the terrace and extend across the terrace to the opposite edge. Two of the molecular wires appear to originate from two nearby points at the step edge, P1 and P2 (marked

https://dx.doi.org/10.1021/acs.jpcc.0c10470
J. Phys. Chem. C 2021, 125, 4223−4234

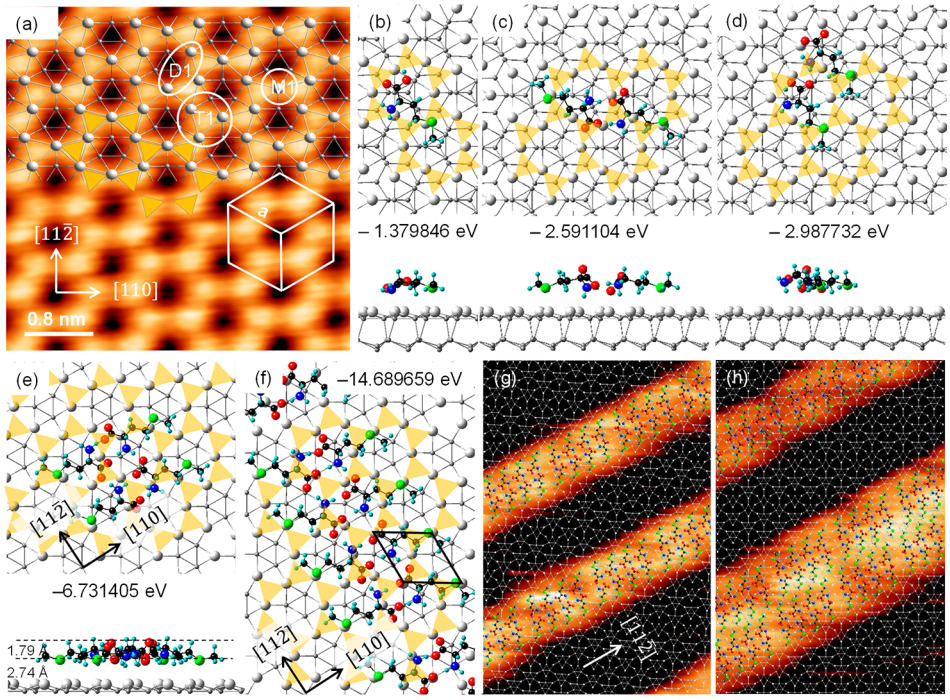

Figure 4. (a) Atomic-resolution empty-state STM image of the Si(111)-$\sqrt{3}\times\sqrt{3}$-Ag surface obtained at a sample bias of +1.6 V with a tunneling current of 0.2 nA at room temperature. The hexagon consists of three $\sqrt{3}\times\sqrt{3}$ surface unit cells, each with two bright protrusions corresponding to two Ag trimers. The optimized structure of the topmost layer of Si(111)-$\sqrt{3}\times\sqrt{3}$-Ag is shown along with the corresponding adsorption sites: atop on a Ag monomer (M1), bridge on a Ag dimer (D1), and threefold hollow on a Ag trimer (T1). (b–f) Optimized equilibrium structures of (b) a methionine molecule adsorbed with an M1-R115 configuration, (c) an antiparallel dimer with the methionine molecules in M1-R43 and M1-R40 configurations, (d) a parallel dimer with methionine in M1-R74 and M1-R57 configurations, (e) a tetramer with methionine in the M1-R125, M1-R115, M1-R115, and M1-R125 configurations, and (f) a periodic model of an extended dimer row. The molecular wire can in effect be considered as four antiparallel dimers adsorbed in a dimer row arrangement along the [11$\bar{2}$] direction (the dimer row growth direction). The total adsorption energies are also indicated in (b–f). Each orange triangle in (b–e) corresponds to a single bright protrusion in the STM image in (a). (g, h) Schematic representations of the calculated dimer rows are superimposed on appropriate STM images to show (g) two separated molecular wires, each containing a single dimer row, and (h) two molecular wires containing (top) a single dimer row and (bottom) a double dimer row (consisting of two single dimer rows side-by-side).

by crosses), and they grow along the directions 60° and 120°, respectively, from the step edge. The molecular wire originating at P1 is found to grow with no change in direction and connects at the other end to another step edge, while the one starting at P2 evidently changes its direction by 120° after a short distance (3–4 nm) and becomes parallel to the wire started at P1 and terminates at the opposite step edge. The growth pattern of these molecular wires suggests that their growth directions critically depend on the $\sqrt{3}\times\sqrt{3}$-Ag surface template. The presence of defects on the $\sqrt{3}\times\sqrt{3}$-Ag template could redirect the growth path of a molecular wire. In Figure 2b1, the larger number of molecular wires along a particular direction may be related to the smaller area of the terrace. In area A4 (Figure 2b1), a short stripe grown on the surface terrace (marked as B) along the dominant direction of the longer stripes is terminated at the junction of another stripe (of nearly the same length) with a 120°-rotated growth direction. Closer examination of this "boomerang" structure in area A4 (Figure 2b2) and of the individual lines in the nanograting in area A5 (Figure 2b3) reveals that a slight change in their adsorption sites to the nearest most favorable adsorption sites could lead to notable defects in the molecular wire. These include bends that redirect the growth direction of the molecular wires, leading to the "boomerang" structure (area A4, Figure 2b2) or kinks in the molecular wires (marked by circles in area A5, Figure 2b3). In Figure 2b4,b5, we overlay schematic models of the dimer rows on the respective STM images of the boomerang structure (Figure 2b2) and kink structure (Figure 2b3) in order to illustrate the effects of the minor underlying imperfections in the nanowire growth. Interestingly, the kinks (or dislocations) in the parallel wires of the nanograting, marked by circles in area A5 (Figure 2b3), all seem to be aligned (and connectable) on a straight line, which suggests the presence of a correlation between the dimer rows that could be related to the confinement of the surface electronic states between the stripes.[40] More details about the molecular configurations of the molecular wires are given in our DFT results discussed below.

Figure 3a shows the STM images of Si(111)-$\sqrt{3}\times\sqrt{3}$-Ag upon a higher exposure of methionine (120 s) collected at 140 K. Evidently, all of the upper-step and lower-step terraces are densely covered with adsorbate islands. The island orientations can be seen more clearly in Figure 3b, which is a magnification of area A1 in Figure 3a. While most of the molecular wires appear to connect to the step edges and antiphase boundaries, not all of the molecular wires initiate the growth at these defect sites. Indeed, the dimer stripes growing along three equivalent directions appear to meet at the interception points forming concentric equilateral triangular nanostructures well inside the terraces. In addition to these concentric triangular nanodomains, nanograting structures (strips of parallel molecular wires) located well inside the terraces (and not connecting to

https://dx.doi.org/10.1021/acs.jpcc.0c10470
J. Phys. Chem. C 2021, 125, 4223–4234

the step edges or antiphase boundaries) are also found when one or more growth directions are disrupted. Other than the increase in the density of these nanostructures, the threefold symmetry of these oriented adsorbate structures remains unchanged from the structures obtained at a lower coverage (Figure 2). At this higher exposure, the step edges and antiphase boundaries are still visible, indicating that the growth of the molecular wires does not extend across and cover these defect structures. However, the extent of long-range order appears to be reduced when the merged stripes of variable orientations grow in close proximity, creating an increased number of intersections. There are no discernible differences in the morphology, density, and distribution of these molecular wire nanostructures between the upper-step terrace and lower-step terrace.

3.3. DFT Modeling of Adsorbed Methionine Monomers, Dimers, Tetramers, and Molecular Wires. To further investigate the dimer-row nanostructures observed in our STM images in more detail, we perform large-scale DFT calculations to discover the optimized equilibrium geometries of plausible adsorption configurations on Si(111)-$\sqrt{3}\times\sqrt{3}$-Ag. Theoretically, there are several possible molecular adsorption configurations for a methionine molecule in contact with the surface, including (a) upright configurations with its head (carboxylic acid) or tail (methyl end) groups pointing to the surface and (b) flat-on configurations where the sulfur atom is either far from the surface atoms, with the methyl end group pointing downward to the surface, or in contact with the surface atoms, with the methyl end group pointing upward toward the vacuum. The upright configuration was observed only for adsorption at higher coverages on Cu(110),[36] on the basis of XPS data that showed the amino and carboxylic acid groups interacting with the surface. All other relevant studies of methionine adsorption on metal surfaces reported the flat-on adsorption configuration parallel to the surface at submonolayer to monolayer coverages on the basis of reflection absorption infrared spectroscopy measurements (on Au(111)[5]), XPS and molecular mechanics data (on Au(111),[5] Ag(111),[3] Cu(111),[6] and graphite[41]) and DFT calculations (on Au(111)[5]). Since we did not observe any discernible shifts in the positions of the XPS spectra upon growth to multilayers and the aforementioned studies showed that the lone-pair electrons of the S atom in the methylthiomethylene group could potentially undergo long-range interactions with the surface states, we orient the methionine molecule in a near flat-on configuration with its S atom pointing to the selected adsorption site.

To determine the most favorable adsorption site, we begin by placing a single methionine molecule in different configurations on adsorption sites of the surface terrace (Figure 4a): Ag monomer (M1) or atop site, Ag dimer (D1) or bridge site, and Ag trimer (T1) or threefold hollow site. For each adsorption site, the molecule is positioned with its long axis (defined in Scheme 1 and with the same color code) rotated around the selected adsorption site counterclockwise from the surface unit cell axis *a*. After geometry optimization, the resulting adsorption configuration is then denoted by the adsorption site and the degree of counterclockwise rotation. A variety of optimized equilibrium adsorption configurations of methionine monomers are shown in Table S2. Figure 4b shows the most stable structure of an isolated methionine molecule adsorbed on the Si(111)-$\sqrt{3}\times\sqrt{3}$-Ag surface near the atop position of a Ag atom (M1) with the long axis rotated 15° counterclockwise from the *a* axis (R15). An adsorption energy (E_{ad}) of −1.38 eV is found for this flat-on adsorption configuration (M1-R15), in which the S and N atoms are located approximately above the two other monomer sites of a Ag trimer with the methyl group lying nearly flat and parallel to the surface. The relatively long Ag−S separation (2.65 Å) and Ag−N separation (2.54 Å) with respect to their respective nominal covalent radii of 2.35 and 2.09 Å[44,45] suggest the presence of dative bonding involving the lone-pair electrons of the S and N atoms with the Ag atoms of the surface. As the dispersion force contribution (−1.09 eV) represents 79% of the calculated adsorption energy (−1.38 eV), the molecule−substrate interaction is governed mainly by van der Waals forces.

Using the most stable zwitterionic structure of the monomer, we optimize the equilibrium adsorption geometries of zwitterionic methionine dimers in antiparallel and parallel configurations, as illustrated in Figures 4c and 4d, respectively. The respective total adsorption energies per molecule for the antiparallel and parallel dimers are −1.29 and −1.49 eV, while the contribution due to dispersion forces per molecule in each dimer is −1.07 eV for the antiparallel configuration and −1.09 eV for the parallel configuration. The energy difference between the dimers most likely originates from the intramolecular stabilization (inside the molecule) via the OH···N hydrogen bonding in the parallel dimer after relaxation. In addition, while the S atoms of both molecules in the dimers are still located on their respective M1 positions, the orientations of the individual molecules in the antiparallel or parallel dimer are different from that in the most stable configuration of the monomer. The adsorption energies and adsorption configurations of single molecules (monomers) are therefore compensated by the intermolecular interactions in the methionine dimers. The optimized geometries of antiparallel and parallel adsorbed methionine dimers with different orientations with respect to the surface are given in Tables S3 and S4, respectively.

On the basis of our STM and XPS results that show extended one-dimensional nanostructures with intermolecular zwitterionic interactions and of previous studies that suggest a universal intermolecular bonding scheme of amino acids on noble metal surfaces,[3,6,43] we search for a stable extended ordered structure of methionine adspecies. We first optimize the geometry of a tetramer (consisting of two antiparallel dimers) oriented along the $[11\bar{2}]$ direction, as shown in Figure 4e. The corresponding adsorption energy per molecule is found to be more negative by 0.30 eV compared with that of the monomer and by 0.39 and 0.19 eV relative to those of the antiparallel and parallel dimers, respectively. This suggests that the formation of an ordered assembly of dimers could further enhance the adsorption stability with respect to the monomer and dimers. To simulate the adsorption configuration of an extended one-dimensional assembly of molecular dimers, a row of four dimers of antiparallel methionine molecules (with eight molecules total in the cell) is placed on a supercell consisting of a 4×4 slab of Si(111)-$\sqrt{3}\times\sqrt{3}$-Ag in the $[11\bar{2}]$ direction. The initial parameters of the dimer row are based on those obtained from the adsorption configurations of the monomer, dimer, and tetramer, where the S atom of each molecule is positioned near an M1 site. Figure 4f shows the optimized structure of the resulting one-dimensional dimer row. Interestingly, the periodicity of the dimer row is in near-perfect registry with that of the slab. The corresponding

https://dx.doi.org/10.1021/acs.jpcc.0c10470
J. Phys. Chem. C 2021, 125, 4223−4234

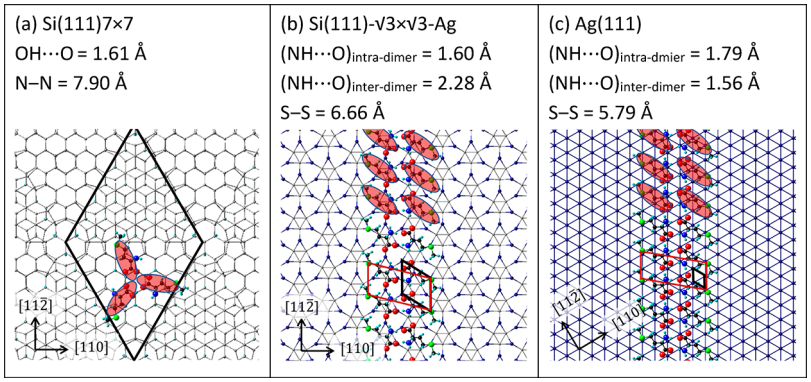

Figure 5. Schematic representations of plausible methionine supramolecular architectures on (a) Si(111)7×7, (b) Si(111)-$\sqrt{3}\times\sqrt{3}$-Ag, and (c) Ag(111) surfaces. The shaded ovals outline the methionine molecules and are used to guide the eyes. The black-lined diamonds in (a–c) show the respective surface unit cells of Si(111)7×7, Si(111)-$\sqrt{3}\times\sqrt{3}$-Ag, and Ag(111), while the red-lined parallelograms in (b) and (c) outline the respective unit cells of the molecular wire on Si(111)-$\sqrt{3}\times\sqrt{3}$-Ag and Ag(111). Relevant structural parameters obtained from DFT-D2 calculations, including the hydrogen-bond lengths and N-to-N and S-to-S separations between two neighboring methionine molecules, are provided at the top of each panel.

calculated adsorption energy is −1.84 eV per molecule, which shows that the ordered structure is stabilized considerably by, on average, 0.46 eV per molecule due to intermolecular interactions. The formation of the ordered dimer rows therefore enhances the adsorption stability with respect to the monomer and dimers. The contribution to the total adsorption energy from the dispersion forces remains essentially unchanged at −1.07 eV (per molecule), and it is still the main stabilizing factor of the dimer row. The separation between the S atom and the underlying Ag atom of the M1 site (2.83 Å) has become larger by 0.18 Å, indicating that the stronger intermolecular interaction in the dimer row could also cause a slight reduction in the molecule–substrate interactions.

To illustrate plausible adsorption configurations of the correlated molecular wires (which are separately aligned in parallel), we superimpose the structures of simulated molecular wires on appropriate STM features in Figure 4g. The width of the calculated molecular wires is found to be in excellent accord with the one measured by STM (Figure 4g), which in turn affirms that the observed molecular wire does indeed correspond to the dimer row structure. To simulate a thicker molecular wire with double width, two dimer rows (with appropriately optimized geometries) are placed side by side on the nearest-neighbor adsorption sites, as shown in Figure 4h. The nearest-neighbor adsorption site for a dimer is defined as an adsorption site where both dimers are adsorbed at equivalent adsorption sites (e.g., M1) with a minimum separation between the innermost methyl groups of the opposite dimer rows. The minimum separation of the carbon atoms of the methyl groups in an end-to-end configuration of an isolated dimer is calculated to be 4.29 Å in our DFT calculations. In the double dimer row model (Figure 4h), this separation is found to be 3.88 Å (on an 8×4 supercell). The proximity of these methyl groups could lead to an increase in the electronic density of states at the center of the double dimers, as exhibited by an increase in the apparent protrusion intensity at the center of the double dimer rows in the STM image (Figure 4h). Indeed, this correlation can be used to explain the intensity profiles of the molecular wire structures observed at higher coverages in our STM results, where a greater number of dimers are located side by side together to form molecular wires of multiple widths (Figure 3). For n increased one-dimensional apparent protrusion intensities (compared with the protrusion intensity at the wire edge), there are n + 1 dimer rows in a unidirectional nanodomain (nanograting) in the STM image (Figure 3b).

3.4. Methionine Adsorption on Si(111)-$\sqrt{3}\times\sqrt{3}$-Ag vs Si(111)7×7 and Ag(111). The formation of supported supramolecular structures depends on both the molecular properties (e.g., molecular size and reactivity) of the adsorbate and the surface properties of the supporting substrate. In general, a delicate balance between the molecule–molecule and molecule–substrate interactions plays a crucial role in determining the formation of any resulting molecular architecture. It is well-known that a low surface diffusion barrier is necessary for a molecule to be able to travel on the surface and interact with other molecules as the initial step in the island growth process. The nucleation points for island formation could be located on terraces, step edges, or other defects. On an ideal terrace, nucleation could occur starting with one molecule if the molecule is large enough (assuming no chemisorption) for the dispersion forces to overcome the kinetic energy of the molecule. For smaller planar molecules, nucleation could occur on a terrace usually with the contribution from more than one molecule. In such a case, the adsorption of the second molecule provides a stabilizing effect on the nucleation process through molecule–molecule attractive interactions. In all of these cases, the nature of the surface (i.e., both its electronic and physical structures) plays a critical role in facilitating diffusion of the molecules. The electronic structure of the surface defines the interactions and types of bonds that are plausible with the adspecies, particularly the strength of the bond between the adspecies and the surface. This in turn affects the diffusivity of the adspecies and determines the self-assembly or self-organization pattern of adspecies on the surface. The geometry of the surface template defines the surface corrugations and, in effect, the separations between adsorption sites, which affect both the diffusivity of adspecies and the geometrical structure of any resulting adsorbate islands. For example, the surface unit cell of the Si(111)7×7 surface corresponds to a diamond-shaped unit cell with a longitudinal length of 46.85 Å (from one corner hole to the opposite corner hole), which is divided into two half unit cells on the basis of their reconstructed symmetry. Each half unit cell is surrounded by the so-called dimer walls

https://dx.doi.org/10.1021/acs.jpcc.0c10470
J. Phys. Chem. C 2021, 125, 4223–4234

with its Si atoms electronically saturated. Each half unit cell is also populated with six Si dangling bonds at the adatom positions, three dangling bonds at the rest atom positions, and one dangling bond shared by the four corner holes (of the unit cell). These dangling bonds provide a set of highly localized adsorption sites for trapping molecules through strong directional covalent bonding. On a semiconductor surface such as Si(111)7×7, the separations between the adsorption sites play a crucial role in the structure of the self-organized architecture because of the directional nature of the dangling bonds. The most favorable adsorption sites for methionine are center adatoms, which are separated from a nearest adatom by 7.65 Å inside the same half unit cell and by 6.77 Å across the dimer wall. Taking advantage of both the electronic effects (particularly, the electrophilic dangling bonds at the adatom sites) and geometry (the spacings between the adatoms and the size of the unit cell) of the surface as well as the attractive intermolecular interactions (hydrogen bonding) and appropriate molecular size (7.4 Å), methionine molecules are found to form Y-shaped clusters inside each half unit cell through N−Si covalent bonding and HO···H intermolecular hydrogen bonding (Figure 5a). However, the formation of a more extended long-range-ordered molecular structure appears to be implausible because the molecule−substrate interactions outweigh the molecule−molecule interactions.[7]

On a metal surface, on the other hand, the electronic structure is not defined by dangling bonds. On the (111) surface of a noble metal such as Ag, the surface electrons exist in the form of a two-dimensional electron gas (2DEG) confined to the first few atomic layers of the crystal, and they play an important role in shaping the physisorption potential. These surface states also contribute to the long-range surface-mediated adsorbate interactions. Indeed, the methionine molecular nanowire gratings formed on Ag(111) have been hypothesized to originate from such long-range surface-mediated interactions.[3,40,46] Together with the two-dimensional electron gas, the smooth corrugation on these surfaces enhances the diffusion properties, making the metal surface a desirable platform for molecular self-assembly. Evidently, we observe a clear distinction between the as-formed supramolecular structures on the Si(111)7×7 surface (zero-dimensional Y-shaped assembly; Figure 5a) and the Ag(111) surface (one-dimensional nanowire assembly; Figure 5c). The Si(111)-$\sqrt{3}\times\sqrt{3}$-Ag surface appears to provide a platform more similar to the Ag(111) surface than to the Si(111)7×7 surface for the self-assembly of methionine molecules (Figure 5b), despite the discernible differences found in the adsorption geometries of the molecular wires on the Si(111)-$\sqrt{3}\times\sqrt{3}$-Ag and Ag(111) surfaces. The surface atom density on Si(111)-$\sqrt{3}\times\sqrt{3}$-Ag (7.83×10^{14} cm^{-2}) is smaller than that on Ag(111) (1.39×10^{15} cm^{-2}). For an ordered supramolecular architecture in registry with the surface, the packing density of methionine molecules should therefore be smaller on the former than the latter surface. The separations between the corresponding adsorption sites (i.e., Ag atop sites) are 6.66 Å on Si(111)-$\sqrt{3}\times\sqrt{3}$-Ag and 5.75 Å on Ag(111) for the adsorbed methionine molecular wires. Given these separations among the adsorption sites, the hydrogen-bond lengths correspond to 2.28 and 1.56 Å along the molecular wire (interdimer) and 1.60 and 1.79 Å across the respective molecular wires (intradimer) on Si(111)-$\sqrt{3}\times\sqrt{3}$-Ag and Ag(111), respectively. Compared with the optimal hydrogen-bond lengths calculated for a molecular wire in the gas phase (1.56 and 1.72 Å along and across the molecular wire), the molecular wire on Si(111)-$\sqrt{3}\times\sqrt{3}$-Ag appears to be less stabilized by intermolecular interactions than that on Ag(111). This difference could account for the easy formation of kinks (and other imperfections) in the molecular wires found on Si(111)-$\sqrt{3}\times\sqrt{3}$-Ag as shown in our STM data.

One major difference between the Si(111)-$\sqrt{3}\times\sqrt{3}$-Ag and Ag(111) surfaces is the high density of step edges (and hence the smaller terrace sizes) and defects on the Si(111)-$\sqrt{3}\times\sqrt{3}$-Ag surface. This influences the molecular wire formation by providing different (perhaps more reactive) adsorption sites for chemisorption of methionine and therefore nucleation points for the growth of nanowires. However, these defect sites disturb the smooth two-dimensional electron gas on the Si(111)-$\sqrt{3}\times\sqrt{3}$-Ag surface and hinder the formation of a unidirectional long-range nanowire grating. In that case, if the goal is to form nanowire gratings on small areas (on a nano- to microscale), one could manipulate the Si(111)-$\sqrt{3}\times\sqrt{3}$-Ag surface preparation procedure to first produce terraces of the desired specific sizes before fabricating the nanogratings. The nucleation of physisorbed methionine islands still takes place on terrace sites mostly because of the attractive intermolecular interactions.

4. CONCLUSION

We have investigated nanofilm growth and interfacial processes of methionine on Si(111)-$\sqrt{3}\times\sqrt{3}$-Ag at room temperature and at 140 K by combining our XPS and STM analyses with large-scale DFT calculations. Adsorption of methionine on a supported two-dimensional metal silicide overlayer like $\sqrt{3}\times\sqrt{3}$-Ag is found to follow the two-stage growth mechanism found on a typical single-crystal metal surface [e.g., Ag(111)] rather than the three-stage growth on a semiconductor surface [e.g., Si(111)7×7]. We observe self-assembly of zwitterionic dimer rows of methionine along the surface close-packed directions at room temperature, which becomes more pronounced and well-defined at low temperature. These results are consistent with our DFT calculations that demonstrate the viability of the formation of methionine dimers and tetramers and the emergence of the dimer row as the molecular wire. The replacement of the thiol group in cysteine by the methylthiomethylene group leads to methionine physisorption (in contrast to chemisorption in the case of cysteine) on the Si(111)-$\sqrt{3}\times\sqrt{3}$-Ag surface. The Si(111)-$\sqrt{3}\times\sqrt{3}$-Ag surface therefore offers a unique platform for developing self-assembled amino acid nanowires, nanogratings, and two-dimensional concentric nanotriangles.

■ ASSOCIATED CONTENT

Supporting Information

The Supporting Information is available free of charge at https://pubs.acs.org/doi/10.1021/acs.jpcc.0c10470.

Binding energies and relative peak areas of spectral features at different exposure times, room-temperature and time-sequenced STM images for 120 s methionine exposure, and various DFT-optimized equilibrium adsorption configurations of methionine monomers and dimers (PDF)

https://dx.doi.org/10.1021/acs.jpcc.0c10470
J. Phys. Chem. C 2021, 125, 4223−4234

AUTHOR INFORMATION

Corresponding Author

Kam Tong Leung − *WATLab and Department of Chemistry, University of Waterloo, Waterloo, Ontario, Canada N2L 3G1;* orcid.org/0000-0002-1879-2806; Email: tong@uwaterloo.ca

Authors

Hanieh Farkhondeh − *WATLab and Department of Chemistry, University of Waterloo, Waterloo, Ontario, Canada N2L 3G1;* orcid.org/0000-0001-6670-3452

Fatemeh R. Rahsepar − *School of Chemistry, College of Science, University of Tehran, Tehran, Iran;* orcid.org/0000-0003-2359-2523

Lei Zhang − *WATLab and Department of Chemistry, University of Waterloo, Waterloo, Ontario, Canada N2L 3G1*

Complete contact information is available at: https://pubs.acs.org/10.1021/acs.jpcc.0c10470

Notes

The authors declare no competing financial interest.

ACKNOWLEDGMENTS

This work was supported by the Natural Sciences and Engineering Research Council of Canada.

REFERENCES

(1) Costa, D.; Pradier, C. M.; Tielens, F.; Savio, L. Adsorption and Self-Assembly of Bio-Organic Molecules at Model Surfaces: A Route towards Increased Complexity. *Surf. Sci. Rep.* **2015**, *70*, 449−553.

(2) Vuyyuri, S. B.; Hamstra, D. A.; Khanna, D.; Hamilton, C. A.; Markwart, S. M.; Campbell, K. C. M.; Sunkara, P.; Ross, B. D.; Rehemtulla, A. Evaluation of D-Methionine as a Novel Oral Radiation Protector for Prevention of Mucositis. *Clin. Cancer Res.* **2008**, *14*, 2161−2170.

(3) Schiffrin, A.; Riemann, A.; Auwarter, W.; Pennec, Y.; Weber-Bargioni, A.; Cvetko, D.; Cossaro, A.; Morgante, A.; Barth, J. V. Zwitterionic Self-Assembly of L-Methionine Nanogratings on the Ag(111) Surface. *Proc. Natl. Acad. Sci. U. S. A.* **2007**, *104*, 5279−5284.

(4) Naitabdi, A.; Humblot, V. Chiral Self-Assemblies of Amino-Acid Molecules: D- and L-Methionine on Au(111) Surface. *Appl. Phys. Lett.* **2010**, *97*, 223112.

(5) Humblot, V.; Tielens, F.; Luque, N. B.; Hampartsoumian, H.; Méthivier, C.; Pradier, C.-M. Characterization of Two-Dimensional Chiral Self-Assemblies L- and D-Methionine on Au(111). *Langmuir* **2014**, *30*, 203−212.

(6) Schiffrin, A.; Reichert, J.; Pennec, Y.; Auwärter, W.; Weber-Bargioni, A.; Marschall, M.; Dell'Angela, M.; Cvetko, D.; Bavdek, G.; Cossaro, A.; Morgante, A.; Barth, J. V. Self-Assembly of L-Methionine on Cu(111): Steering Chiral Organization by Substrate Reactivity and Thermal Activation. *J. Phys. Chem. C* **2009**, *113*, 12101−12108.

(7) Rahsepar, F. R.; Leung, K. T. Self-Organized Supported Clusters of L-Methionine. *J. Phys. Chem. C* **2016**, *120*, 6534−6542.

(8) Kühnle, A. Self-Assembly of Organic Molecules at Metal Surfaces. *Curr. Opin. Colloid Interface Sci.* **2009**, *14*, 157−168.

(9) Belianinov, A. A. Ag on Si(111) from Basic Science to Application. Doctoral Dissertation, Iowa State University, Ames, Iowa, 2012.

(10) Johansson, L. S. O.; Landemark, E.; Karlsson, C. J.; Uhrberg, R. I. G. Fermi-Level Pinning and Surface-State Band Structure of the Si(111)-($\sqrt{3}\times\sqrt{3}$)R30°-Ag. *Phys. Rev. Lett.* **1989**, *63*, 2092−2095.

(11) Hasegawa, S.; Tong, X.; Jiang, C. S.; Nakajima, Y.; Nagao, T. Electrical Conduction via Surface-State Bands. *Surf. Sci.* **1997**, *386*, 322−327.

(12) Hasegawa, S.; Sato, N.; Shiraki, I.; Petersen, C. L.; Bøggild, P.; Hansen, T. M.; Nagao, T.; Grey, F. Surface-State Bands on Silicon −Si(111)-$\sqrt{3}\times\sqrt{3}$-Ag Surface Superstructure−. *Jpn. J. Appl. Phys.* **2000**, *39*, 3815−3822.

(13) Upward, M. D.; Beton, P. H.; Moriarty, P. Adsorption of Cobalt Phthalocyanine on Ag Terminated Si(111). *Surf. Sci.* **1999**, *441*, 21−25.

(14) Butcher, M. J.; Nolan, J. W.; Hunt, M. R. C.; Beton, P. H.; Dunsch, L.; Kuran, P.; Georgi, P.; Dennis, T. J. S. Orientationally Ordered Island Growth of Higher Fullerenes on Ag/Si(111)-($\sqrt{3}\times\sqrt{3}$)-R30°. *Phys. Rev. B: Condens. Matter Mater. Phys.* **2001**, *64*, 195401.

(15) Theobald, J. A.; Oxtoby, N. S. N. S.; Phillips, M. A.; Champness, N. R. N. R.; Beton, P. H. Controlling Molecular Deposition and Layer Structure with Supramolecular Surface Assemblies. *Nature* **2003**, *424*, 1029−1031.

(16) Guaino, P.; Carty, D.; Hughes, G.; Moriarty, P.; Cafolla, A. A. Scanning Tunneling Microscopy Study of Pentacene Adsorption on Ag/Si(111)-($\sqrt{3}\times\sqrt{3}$)R30°. *Appl. Surf. Sci.* **2003**, *212*−*213*, 537−541.

(17) Sheerin, G.; Cafolla, A. A. Self-Assembled Structures of Trimesic Acid on the Ag/Si(111)-($\sqrt{3}\times\sqrt{3}$)R30° Surface. *Surf. Sci.* **2005**, *577*, 211−219.

(18) Perdigão, L. M. a; Champness, N. R.; Beton, P. H. Surface Self-Assembly of the Cyanuric Acid-Melamine Hydrogen Bonded Network. *Chem. Commun.* **2006**, 538−540.

(19) Perdigão, L. M. A.; Staniec, P. A.; Champness, N. R.; Kelly, R. E. A.; Kantorovich, L. N.; Beton, P. H. Experimental and Theoretical Identification of Adenine Monolayers on Ag-Terminated Si(111). *Phys. Rev. B: Condens. Matter Mater. Phys.* **2006**, *73*, 195423.

(20) Gustafsson, J. B.; Zhang, H. M.; Moons, E.; Johansson, L. S. O. Electron Spectroscopy Studies of PTCDA on Ag/Si(111)-$\sqrt{3}\times\sqrt{3}$. *Phys. Rev. B: Condens. Matter Mater. Phys.* **2007**, *75*, 155413.

(21) Beggan, J. P.; Krasnikov, S. A.; Sergeeva, N. N.; Senge, M. O.; Cafolla, A. A. Self-Assembly of Ni(II) Porphine Molecules on the Ag/Si(111)-($\sqrt{3}\times\sqrt{3}$)R30° Surface Studied by STM/STS and LEED. *J. Phys.: Condens. Matter* **2008**, *20*, 015003.

(22) Li, Q.; Yamazaki, S.; Eguchi, T.; Kim, H.; Kahng, S.-J.; Jia, J.-F.; Xue, Q.-K.; Hasegawa, Y. Initial Adsorption and Kondo Resonance of 5,10,15,20-Tetrakis(4-bromophenyl)porphyrin−Co Molecules on Ag/Si(111) Surface Studied by Low-Temperature Scanning Tunneling Microscopy/Spectroscopy. *Jpn. J. Appl. Phys.* **2009**, *48*, 08JB01.

(23) Yokoyama, T.; Kawasaki, M.; Asari, T.; Ohno, S.; Tanaka, M.; Yoshimoto, Y. Adsorption and Self-Assembled Structures of Sexithiophene on the Si(111)-$\sqrt{3}\times\sqrt{3}$-Ag Surface. *J. Chem. Phys.* **2015**, *142*, 204701.

(24) Liu, R.; Fu, C.; Perepichka, D. F.; Gallagher, M. C. Supramolecular Structures of Halogenated Oligothiophenes on the Si(111)-$\sqrt{3}\times\sqrt{3}$-Ag Surface. *Surf. Sci.* **2016**, *647*, 51−54.

(25) Suzuki, T.; Lutz, T.; Payer, D.; Lin, N.; Tait, S. L.; Costantini, G.; Kern, K. Substrate Effect on Supramolecular Self-Assembly: From Semiconductors to Metals. *Phys. Chem. Chem. Phys.* **2009**, *11*, 6498−6504.

(26) Farkhondeh, H.; Rahsepar, F. R.; Zhang, L.; Leung, K. T. Structural and Chemical Evolution of L-Cysteine Nanofilm on Si(111)-$\sqrt{3}\times\sqrt{3}$-Ag: From Preferential Growth at Step Edges and Antiphase Boundaries at Room Temperature to Adsorbate-Mediated Metal Cluster Formation at Elevated Temperature. *Langmuir* **2019**, *35*, 16185−16200.

(27) Wan, K. J.; Lin, X. F.; Nogami, J. Surface Reconstructions in the Ag/Si(111) System. *Phys. Rev. B: Condens. Matter Mater. Phys.* **1993**, *47*, 13700−13712.

(28) Wallace, W. E. Mass Spectra. In *NIST Chemistry Webbook, NIST Standard Reference Database Number 69*; Linstrom, P. J., Mallard, W. G., Eds.; National Institute of Standard and Technology: Gaithersburg MD; Vol. *20899*.

(29) Horcas, I.; Fernández, R.; Gómez-Rodríguez, J. M.; Colchero, J.; Gómez-Herrero, J.; Baro, A. M. WSXM: A Software for Scanning

Probe Microscopy and a Tool for Nanotechnology. *Rev. Sci. Instrum.* **2007**, *78*, 013705.
(30) Blöchl, P. E.; Jepsen, O.; Andersen, O. K. Improved Tetrahedron Method for Brillouin-Zone Integrations. *Phys. Rev. B: Condens. Matter Mater. Phys.* **1994**, *49*, 16223−16233.
(31) Kresse, G.; Joubert, D. From Ultrasoft Pseudopotentials to the Projector Augmented-Wave Method. *Phys. Rev. B: Condens. Matter Mater. Phys.* **1999**, *59*, 1758−1775.
(32) Perdew, J. P.; Burke, K.; Ernzerhof, M. Generalized Gradient Approximation Made Simple. *Phys. Rev. Lett.* **1996**, *77*, 3865−3868.
(33) Grimme, S. Semiempirical GGA-Type Density Functional Constructed with a Long-Range Dispersion Correction. *J. Comput. Chem.* **2006**, *27*, 1787−1799.
(34) Rahsepar, F. R.; Moghimi, N.; Leung, K. T. Surface-Mediated Hydrogen Bonding of Proteinogenic α-Amino Acids on Silicon. *Acc. Chem. Res.* **2016**, *49*, 942−951.
(35) Clark, D. T.; Peeling, J.; Colling, L. An Experimental and Theoretical Investigation of the Core Level Spectra of a Series of Amino Acids, Dipeptides and Polypeptides. *Biochim. Biophys. Acta, Protein Struct.* **1976**, *453*, 533−545.
(36) Méthivier, C.; Humblot, V.; Pradier, C. M. L-Methionine Adsorption on Cu(110), Binding and Geometry of the Amino Acid as a Function of Coverage. *Surf. Sci.* **2015**, *632*, 88−92.
(37) Rahsepar, F. R.; Leung, K. T. Surface Functionalization of Reconstructed Si(111) with Methionine. *J. Phys. Chem. C* **2019**, *123*, 26980−26988.
(38) McComb, D. W.; Wolkow, R. A.; Hackett, P. A. Defects on the Ag/Si(111)-($\sqrt{3}\times\sqrt{3}$) Surface. *Phys. Rev. B: Condens. Matter Mater. Phys.* **1994**, *50*, 18268−18274.
(39) Shibata, A.; Kimura, Y.; Takayanagi, K. On the Restructured Layer of the Si(111)$\sqrt{3}\times\sqrt{3}$-Ag Structure Studied by Scanning Tunneling Microscopy. *Surf. Sci.* **1992**, *275*, L697−L701.
(40) Pennec, Y.; Auwärter, W.; Schiffrin, A.; Weber-Bargioni, A.; Riemann, A.; Barth, J. V. Supramolecular Gratings for Tuneable Confinement of Electrons on Metal Surfaces. *Nat. Nanotechnol.* **2007**, *2*, 99−103.
(41) Riemann, A.; Nelson, B. Molecular Wires Self-Assembled on a Graphite Surface. *Langmuir* **2009**, *25*, 4522−4525.
(42) Krebs, E.; Grabill, L.; Riemann, A. Amino Acid Nanopatterning on Graphite. *Surf. Sci.* **2018**, *678*, 143−148.
(43) Reichert, J.; Schiffrin, A.; Auwärter, W.; Weber-Bargioni, A.; Marschall, M.; Dell'Angela, M.; Cvetko, D.; Bavdek, G.; Cossaro, A.; Morgante, A.; Barth, J. V. L-Tyrosine on Ag(111): Universality of the Amino Acid 2D Zwitterionic Bonding Scheme? *ACS Nano* **2010**, *4*, 1218−1226.
(44) Orpen, A. G.; Brammer, L.; Allen, F. H.; Kennard, O.; Watson, D. G.; Taylor, R. Tables of Bond Lengths Determined by X-Ray and Neutron Diffraction. Part 2. Organometallic Compounds and Co-Ordination Complexes of the d- and f-Block Metals. *J. Chem. Soc., Dalton Trans.* **1989**, S1−S83.
(45) Cordero, B.; Gómez, V.; Platero-Prats, A. E.; Revés, M.; Echeverría, J.; Cremades, E.; Barragán, F.; Alvarez, S. Covalent Radii Revisited. *J. Chem. Soc. Dalt. Trans.* **2008**, 2832−2838.
(46) Urgel, J. I.; Vijayaraghavan, S.; Ecija, D.; Auwärter, W.; Barth, J. V. Tetracene Confinement in L-Methionine Gratings on the Ag(111) Surface. *Surf. Sci.* **2016**, *643*, 87−90.

https://dx.doi.org/10.1021/acs.jpcc.0c10470
J. Phys. Chem. C 2021, 125, 4223−4234